

Quantum Dots

A Millifluidic Reactor System for Multistep Continuous Synthesis of InP/ZnSeS Nanoparticles

Ajit Vikram⁺,^[a] Vivek Kumar⁺,^[a] Utkarsh Ramesh,^[a] Karthik Balakrishnan,^[a] Nuri Oh,^[b] Kishori Deshpande,^[c] Trevor Ewers,^[d] Peter Trefonas,^[e] Moonsub Shim,^[b] and Paul J. A. Kenis^{*[a]}

Abstract: Despite the growing interest in quantum dots for applications ranging from bioimaging to display technologies, the reproducible and high-quality synthesis of Cd-free quantum dots (QDs) on a large scale remains challenging. Conventional large-scale batch synthesis techniques are limited by slow precursor heating/cooling/mixing, poor reproducibility and low productivity. In recent years, the continuous flow synthesis of QDs using microfluidic approaches has shown promise to overcome the shortcomings of batch synthesis. However, the application of microfluidic reactors for synthesis of Cd-free QDs exhibiting high photoluminescence quantum yield (PL QY) at high production rate remains a challenge. Here, we report a modular millifluidic

reactor for the fully continuous multi-step synthesis of InP/ZnSeS core-shell QDs, that integrates the precise control over reaction conditions with the potential for gram-scale production rates. We use a design of experiment approach to understand and optimize the process parameters for the synthesis, resulting in PL QY up to 67% with good reproducibility in terms of both QY and peak position (less than 5% standard deviation). Additionally, by changing the process parameters for different reaction stages (core and shell reactors), the wavelength of the InP/ZnSeS particles can be tuned to cover nearly the entire visible spectrum (480–650 nm).

1. Introduction

Colloidal quantum dots (QD) are of significant promise for many applications including, optoelectronics,^[1] photocatalysis,^[2] and biolabelling and bioimaging^[3] due to their size and composition dependent, and thus tunable, optoelectronic properties. CdSe has received most attention among various semiconductor nanoparticle compositions.^[4] Despite their advantages – high quantum yield, narrow full-width-at-half-maximum (FWHM), and high photostability, the potential of Cd-

based nanoparticles in commercial products is limited due to their high toxicity.^[5,6] Consequently, the interest of academia and industry has shifted towards identification of Cd-free alternatives such as InP QDs that also exhibit tunable emission wavelength, but are significantly less toxic.^[7] Many InP based core-shell QDs and associated batch synthesis processes have been reported in the literature, including InP/ZnS,^[8] InP/ZnSe/ZnS,^[9] InP/ZnSeS,^[10] and ZnSe/InP/ZnS.^[11] Among these, InP/ZnSeS particles exhibit high photometric performance with narrow emission FWHM of less than 60 nm and PL QYs as high as 80% for green-emission.^[10] The integration of a ZnSe shell, preferentially grown close to the InP core particles, along with a ZnS shell results in high photo/chemical stability as well as high quantum yield core-shell nanoparticles due to alleviated lattice strain.^[10] The addition of zinc precursors during the core growth step has also been shown to be a critical step for synthesis of high quality InP nanoparticles.^[12] The zinc precursor results in formation of a stable intermediate Zn-P bond, thus lowering its reactivity. The low reactivity enables slow growth rate, resulting in more monodisperse InP QDs. Similarly, mechanistic studies to understand the role of precursor conversion rates,^[13] fatty acids,^[14] alternate phosphorous precursors like phosphine gas,^[15] white phosphorous,^[16] tris(trimethylgermanyl)phosphine,^[13] and aminophosphines,^[17] in the synthesis of InP QDs have been reported in recent years. A recent review by Reiss *et al.* nicely summarizes the role of the aforementioned and other factors involved in the synthesis of InP QDs in detail.^[18]

[a] A. Vikram,⁺ V. Kumar,⁺ U. Ramesh, K. Balakrishnan, Prof. P. J. A. Kenis
Department of Chemical & Biomolecular Engineering
University of Illinois at Urbana-Champaign
600 South Mathews Avenue, Urbana, IL 61801, USA
E-mail: kenis@illinois.edu


[b] N. Oh, Prof. M. Shim
Materials Science and Engineering
University of Illinois at Urbana-Champaign
1304 West Green Street, Urbana, IL 61801, USA

[c] Dr. K. Deshpande
The Dow Chemical Company
230 Abner Jackson Pkwy/H.H.Dow/2 A185, Lake Jackson, TX 77566, USA

[d] Dr. T. Ewers
The Dow Chemical Company
1707 Building, Midland, MI 48640, USA

[e] Dr. P. Trefonas
Dow Electronic Materials
455 Forest Street, Marlborough, MA 01752, USA

[*] Both authors contributed equally.

 Supporting information for this article is available on the WWW under <https://doi.org/10.1002/cnma.201800160>

Despite significant progress in the development of batch synthesis techniques for In-based nanoparticles, the use of continuous flow microreactors recently has emerged as a more promising system for the synthesis of high quality colloidal QDs.^[19] Compared to conventional batch methods, flow reactors have the potential to produce QDs with narrower size distribution and higher reproducibility due to their superior ability to control reaction conditions (e.g., heating/cooling, residence times).^[20] Since the optical properties of the semiconductor nanomaterials vary depending on choice of composition, band alignment, etc., a direct comparison is not entirely fair. However, for any given nanomaterial composition, due to superior control of reaction conditions in continuous flow reactors compared to large-scale batch reactors, materials with better optical properties can be synthesized in flow reactors. For example, Nightingale *et al.* reported the first application of microreactors for the synthesis of size-tunable InP quantum dots with a FWHM of 80 nm.^[19a] Since then, several insightful works have been reported on the application of microfluidics to understand the underlying mechanism involved in formation and growth of InP nanoparticles.^[19b,d,21] However, to date none of these continuous flow approaches have been able to produce In-based QDs with high PL. Furthermore, the majority of these microreactor approaches is hampered by low production rates, and scaling up while retaining similar control over heat and mass transfer during mixing and reaction is challenging.^[20]

Millifluidic flow reactor designs may offer an alternative approach to transfer QD synthesis from batch to a scalable continuous flow approach. In recent years, millifluidic reactor (reactors with channel diameter > 1 mm) systems have been implemented for nanomaterials synthesis including copper,^[22] silver,^[23] and gold^[24] at high production rate. However, application of millifluidic reactors for synthesis of semiconductor-based quantum dots has received only little attention.^[25] Kim *et al.* implemented a hybrid reactor system, utilizing a millifluidic reactor to synthesize InP/ZnS core-shell particles.^[25a] However, the reactor setup used in aforementioned work is not fully continuous: it is a hybrid of a semi-batch and a flow reactor. The shell precursors were mixed in a manner similar to a typical batch synthesis that does not allow good control over mixing with respect to the rate of mixing and temperature. Moreover, the synthesized nanoparticles were reported to exhibit a maximum PL QY of only 37% and 20% for particles emitting in the red and green regions respectively, which is still significantly less than what has been achieved via batch synthesis. Previously, we have reported large-scale synthesis of CdSe with PL QYs over 60% using a continuous flow stainless steel tube reactor.^[25b] However, the reactor configuration, comprised of a 2.2 mm diameter coiled stainless steel tube, used in this study is not suitable for air-sensitive reactions (for instance, InP synthesis) and the maximum operating temperature is limited by the decomposition temperature of the oil used for heating. More importantly, the reactant streams in the reactor used for CdSe synthesis, were cooled using an open-air cooling design (collection in a vial), resulting in unwanted particle growth. A subsequent modular design improved the

ability to control heating and cooling rates. Rapid heating of the reactant stream was achieved by using an electrically heated reactor that consists of a stainless steel coil wrapped around a graphite core inserted in a stainless steel housing that also holds heating cartridges. In addition, a heat exchanger cooling module was used for rapid cooling of the product streams. Using this reactor setup, we reported continuous flow single step synthesis of anisotropic ZnSe and CdSe/ZnS nanorods that exhibited PL QYs of over 30%.^[25c] Despite the improved control over reaction heating/cooling, both of our previously reported reactor designs were limited by a broad residence time distribution inside the reactors (due to a parabolic flow profile). Furthermore, for multistep synthesis of for example core-shell particles, the core product of a first continuous flow step and the shell precursors had to be mixed manually in a flask before that reactant mixture could be used in a second continuous flow step for shell formation. Apart from being cumbersome and not being truly continuous, this procedure (especially due to inefficient mixing) also negatively affected the quality of the resulting core-shell particles.

Here, we demonstrate a modular millifluidic continuous flow reactor design that minimizes residence time distribution and enhances control over reaction conditions. The modular design is comprised of two or more distinct reactors for core formation and subsequent shell growth, connected in series with cooling modules for rapid cooling of product and one or more inline mixing units for uniform and fast mixing at controlled temperature outside of the reactor units. Furthermore, the incorporation of static mixers inside the reactor modules minimizes the residence time distribution as it breaks up the parabolic flow profile. This continuous flow design is utilized for the synthesis of InP/ZnSeS core/shell QDs that cover nearly the entire visible range upon variation of the residence time, temperature, and precursor concentration. A systematic design of experiment approach helped to optimize the process parameters for continuous synthesis, resulting in the synthesis of QDs exhibiting PL QY exceeding 60%.

2. Results and Discussion

2.1. Reactor Setup

Figure 1 shows the schematic of the continuous flow system with two identical reactor modules, two cooling modules, and an inline mixer. The entire setup, including the precursor flasks and the product collection vial, can be operated under inert conditions.

The **reactor modules** (Figure 2a) are fabricated from a 6.4 cm thick, 12.7 cm long (core reactor) and 13.9 cm long (shell reactor) stainless steel cylindrical bar that have a flow channel of 7.2 mm in diameter and a volume of 5.2 mL (core reactor) and 5.7 mL (shell reactor) through their center (Figure 2b) in which a mixer element (Figure 2b) is placed. The reactor is heated by four symmetrically placed cartridge heaters around the reactor channel (Figure 2b). The stainless steel reactor, due to the electrical heating by cartridge heaters, allows the

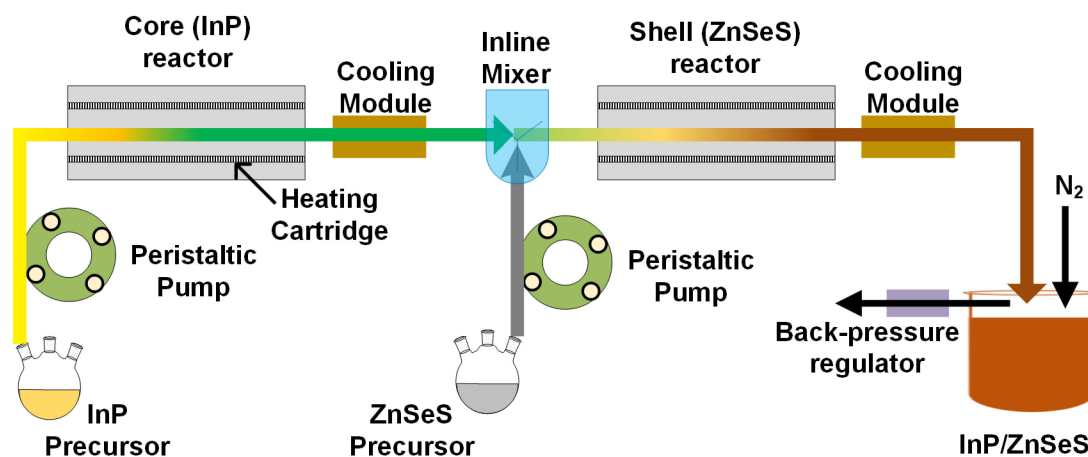


Figure 1. Schematic of the modular continuous flow reactor system for InP/ZnSeS synthesis. The design includes a core and a shell reactor, cooling modules and an inline mixer and is operated under inert conditions.

reactant fluid to be uniformly and rapidly heated from 25 to 270 °C, a major improvement over batch synthesis and oil-bath based flow reactors.^[25c] The heat transfer to the reactant fluid entering the reactor, as a function of flow rate, was investigated using a COMSOL based model. The temperature profile inside the reactor revealed that the reactant streams can be heated from 25 to 270 °C within 0.5–30 seconds, depending on the operating flow rate of 0.1–5 mL/min (Figure S5). The entire reactor module is insulated using ceramic wool and layers of ceramic roll to avoid drastic temperature gradients within the setup (see Figure S1 for photograph of the actual setup). The InP precursor mixture containing indium myristate, Tris(trimethylsilyl)phosphine, and zinc oleate in octadecene as the solvent is kept in a well-stirred three-neck flask (core precursor flask) at 50 °C, which is a low enough temperature to avoid any unwanted reaction.^[26] To initiate core growth, the core precursor mixture is pumped at a flow rate of 0.1 to 5 mL/min through the first reactor module (core reactor) at a desired core growth temperature (210–230 °C). Upon exiting the core reactor, the product stream is cooled to room temperature (RT) by passing through a **cooling module**, installed downstream of the reactor to ensure rapid quenching (in < seconds) of the product temperature to avoid any residual reaction.^[25c] After cooling to RT, the product stream containing zinc oleate passivated InP core nanoparticles from the core reactor is then mixed in an **inline mixer** with the shell precursor solution, prepared in a separate flask (shell precursor flask), where zinc oleate, the selenium precursor (trioctylphosphine-Se, TOP-Se), and the sulfur precursor (1-dodecanethiol, 1-DDT) are kept well-stirred at 120 °C. The mixed stream then enters the second reactor module (shell reactor) at a desired temperature (290–310 °C), to induce ZnSeS shell passivation. The inline mixer contains 5 stainless steel mixing elements, each 4.8 mm wide and 4.8 mm long. The set of mixing elements are designed to promote effective mixing between incoming streams of InP product and ZnSeS precursors.^[27] The mixer is also heated using a rope heater to control the mixing temperature of the two streams. The flow line (shell precursor stream) and inline mixer

are kept at 90 °C to maintain a uniform mixing temperature. The final product solution containing ZnSeS-passivated InP cores is collected in an air-tight vial after passing through a cooling module. The helical **static mixers** inside both the reactor channels (Figure 2b) break the parabolic flow front of the reactant stream to ensure a narrow residence time distribution (RTD). A step-input tracer experiment, conducted to characterize the RTD of the reactor, shows a very narrow spread in RTD curve with low dispersion at an average residence time of 5.2 minutes in the reactor (Figure S4). The details of the tracer experiment have been included in supporting information. In addition to minimizing the parabolic flow of reactant streams, the stainless steel static mixer also

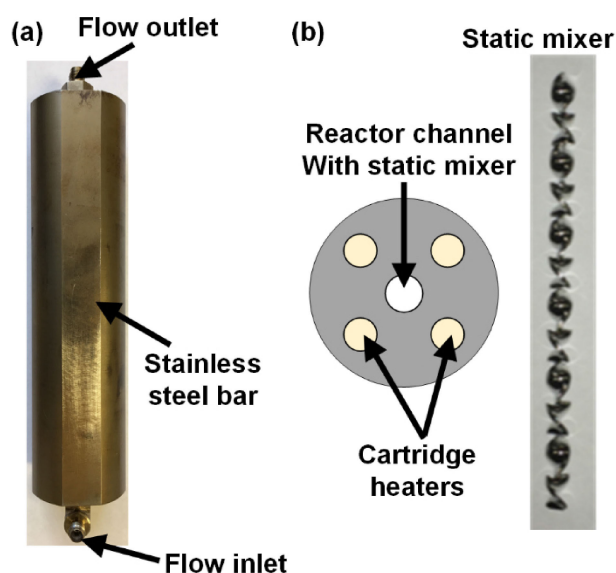


Figure 2. Reactor module design. (a) Photograph of fabricated stainless-steel reactor module with a channel inlet and outlet. (b) Cross-sectional view of reactor module, with cartridge heaters placed symmetrically around the channel (central hole) for uniform heating, and static mixer present inside the reactor channel.

facilitates heat flow within the channel. In summary, we expect that the enhanced control over fast and uniform heating, cooling, and mixing throughout the modular setup (within the reactors as well as within the inline mixer), will result in highly reproducible synthesis of core-shell quantum dots with desired optical properties.

2.2. Synthesis of InP/ZnSeS Nanoparticles

Utilizing the aforementioned modular continuous flow reactor system, we synthesized InP/ZnSeS nanoparticles by first synthesizing Zn(OA)₂ passivated InP cores followed by a shell growth step, without interruption (no purification of core product before shell passivation). While typically TOP-S is used as the sulfur precursor for shell growth, prior work has reported DDT as a more effective sulfur precursor for ZnSeS alloyed shell passivation.^[10b] DDT is less reactive than TOP-S, therefore TOP-Se is expected to preferentially grow over core surface before DDT resulting in a higher concentration of ZnSe shell coating around InP cores. From prior work on elemental mapping of the ZnSeS shell, it is known that the concentration of ZnSe gradually decreases with increasing distance from the InP core particles: InP QDs with a thin shell of ZnSe close to the core and a thick ZnS shell farther away from the core.^[10] These QDs are expected to exhibit higher PL and photostability since they combine the benefits of reduced lattice strain (only 3.4% for ZnSe shell, compared to 8.5% for ZnS shell) with the enhanced passivation characteristics of a ZnS shell.

To confirm successful incorporation of Se, we also synthesized a control sample: InP/ZnS quantum dots (lacking Se). Figure 3 shows the fluorescence spectra for Zn(OA)₂-passivated

InP core nanoparticles, the ZnS and ZnSeS shell passivated core/shell quantum dots, synthesized at a core reactor temperature of 230 °C, a shell reactor temperature of 310 °C and a residence time of 9 minutes in the core reactor. The red shift of 26 nm in PL peak position upon shell passivation indicates the successful synthesis of a core-shell structure. The presence of ZnSe in the shell is further supported by a smaller red-shift of 14 nm (see Figure 3) with ZnS-only shell growth (peak wavelength – 616 nm) using similar reaction conditions. A similar trend has been previously reported for InP/ZnS and InP/ZnSe, where the ZnSe shell leads to a larger red-shift in the PL peak position than ZnS shell.^[10a] The presence of ZnSe in the final product is further supported by the EDS analysis of the synthesized product (Figure S7).

2.3. Design of Experiment Study

The synthesized InP/ZnSeS QDs exhibited 41% quantum yield with FWHM of 83 nm (Figure 3). To further optimize the reaction conditions and understand the sensitivity of four different process parameters including (1) core reactor temperature, (2) shell reactor temperature, (3) residence time in core reactor, and (4) shell precursor concentration, a systematic mixed-level factorial design of experiment (DOE) study was opted. Table S1 shows the levels for different process parameters included in the DOE. The process parameters were mutually varied to optimize PL QY and emission wavelength of the InP/ZnSeS quantum dots. Due to the relatively large FWHM for red-emitting particle, and hence the lack of a distinct absorption peak, only the PL emission peak and the QY are used to quantify the emission properties of the final products. We do not include FWHM as a critical parameter for DOE optimization, due to relatively small change (80–90 nm) with variation in most of the process parameters. The shell precursor concentration was quantified by [Zn]:[In] ratio, where [Zn] and [In] are concentration of Zn-oleate in shell precursor stream and that of In-myristate in core precursor stream, respectively. For the typical synthesis reported in the rest of this paper, the core and shell reactor temperatures were kept at 230 °C and 310 °C, respectively, [Zn]:[In] ratio of 15:1 was used, and the residence time of 45 minute in the core reactor was maintained, unless specified otherwise.

Effect of flow rate: Figure 4a and 4b shows the transmission electron microscopy (TEM) images of core-shell QDs synthesized at residence time of 30 minute (62% QY). The average particle size for InP/ZnSeS based on the TEM image was 5.9 nm with standard deviation of 1.2 nm from analysis of 250 nanoparticles (Figure 4c). Figure 4d shows the PL spectra of the InP/ZnSeS products corresponding to different core reactor residence time. The flow rate of InP product stream and shell precursor stream was kept the same, restricting residence time for shell growth to nearly half of the core growth residence time. The Zn(OA)₂-passivated InP core particles (shown in blue in Figure 3) synthesized at a residence time of 9 minute showed a significant red shift from 599 nm to 626 nm upon ZnSeS shell passivation (shown in blue in Figure 4d). The PL spectra of the

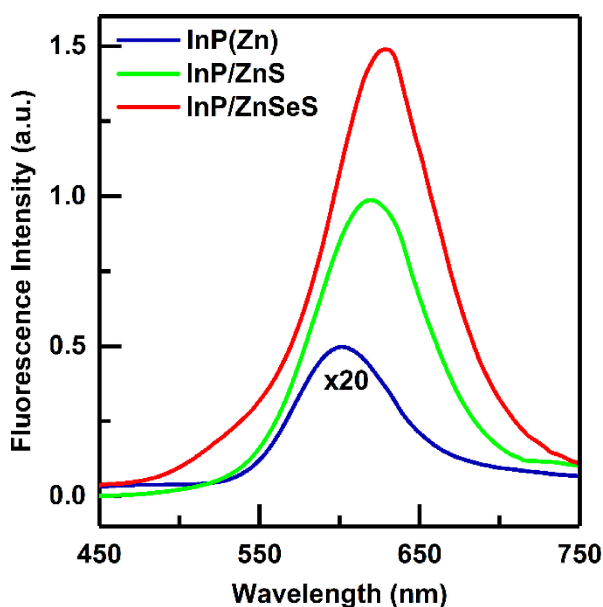


Figure 3. Effect of ZnSeS shell. Photoluminescence spectra of Zn(OA)₂-passivated InP (peak – 602 nm), InP/ZnS (peak – 616 nm) and InP/ZnSeS (peak – 628 nm). The curve for Zn(OA)₂-passivated InP core has been shown 20 times higher for clarity of the peak location.

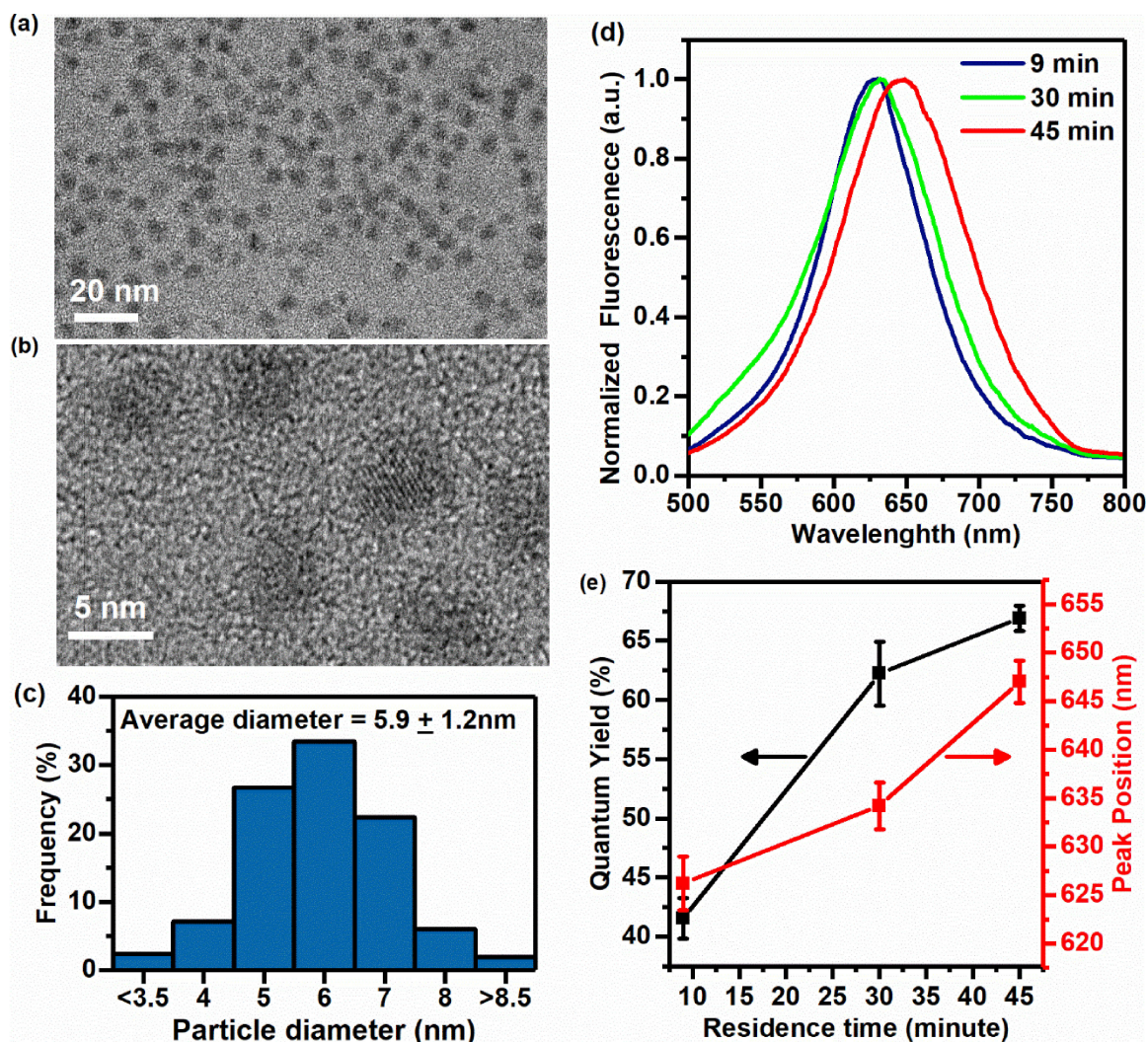


Figure 4. Effect of varying residence time. (a-b) TEM images of InP/ZnSeS synthesized at residence time of 30 minutes, scale bar: 20 nm in (a) and 5 nm in (b) (QY – 67% and PL peak – 646 nm). (c) Particle size distribution obtained from analyzing 250 particles shows a mean diameter of 5.9 nm with 1.2 nm standard deviation. (d) Fluorescence spectra, and (e) Quantum yield and peak position (arrows shown for visual clarity of axis) for InP/ZnSeS synthesized at varying residence time (9 minutes, 30 minutes and 45 minutes) in core reactor. The error bars represent one standard deviation in QY and PL peak based on 5 experiments at each residence time. All the results shown are based on core reactor at 230 °C and shell reactor at 310 °C.

InP/ZnSeS products exhibited a red shift of 22 nm upon further increasing the residence time from 9 minute to 45 minute (Figure 4d). The core particles exhibited only small changes in terms of optical properties (both absorbance and PL peak position) upon variation of the core growth residence time from 9 to 45 minutes (Figure S6) and hence the change in overall PL properties of the final products can be attributed to the shell passivation effect only.

The PL QY of the shell passivated nanoparticles increased with increasing residence time, from 40% at 9 minute to 67% at 45 minute (Figure 4e). Such trend is attributed to a more effective shell formation at lower flow rates (higher residence times). Increasing the core growth residence time beyond 45 minutes yields products with poor fluorescence, possibly due to over-ripening of the particles. The error bars shown in Figure 4e represent one standard deviation from average PL QY and peak position for nanoparticles synthesized at varying

residence time (less than 5% for both QY as well as peak position). These results further confirm a key advantage of continuous flow synthesis for high reproducibility due to better control over the quality of the product and thus the spectral characteristics, which is a major improvement over conventional batch synthesis technique that can suffer significantly from batch-to-batch variation in product quality.

Effect of reactor temperatures: In the next step, the effect of reactor temperatures on InP/ZnSeS growth and PL properties was studied. Figure 5 shows the interplay of both core and shell reactor temperature on the PL of the different products. Increase in both core and shell reactor temperature resulted in a small red shift and a higher QY in the final product. However, the final product seems to be more sensitive to core reactor temperature: A more than two-fold increase in QY from 31% to 67% (Figure 5b) in combination with a small red shift of 8–12 nm (Figure 5c) was observed when the core temperature

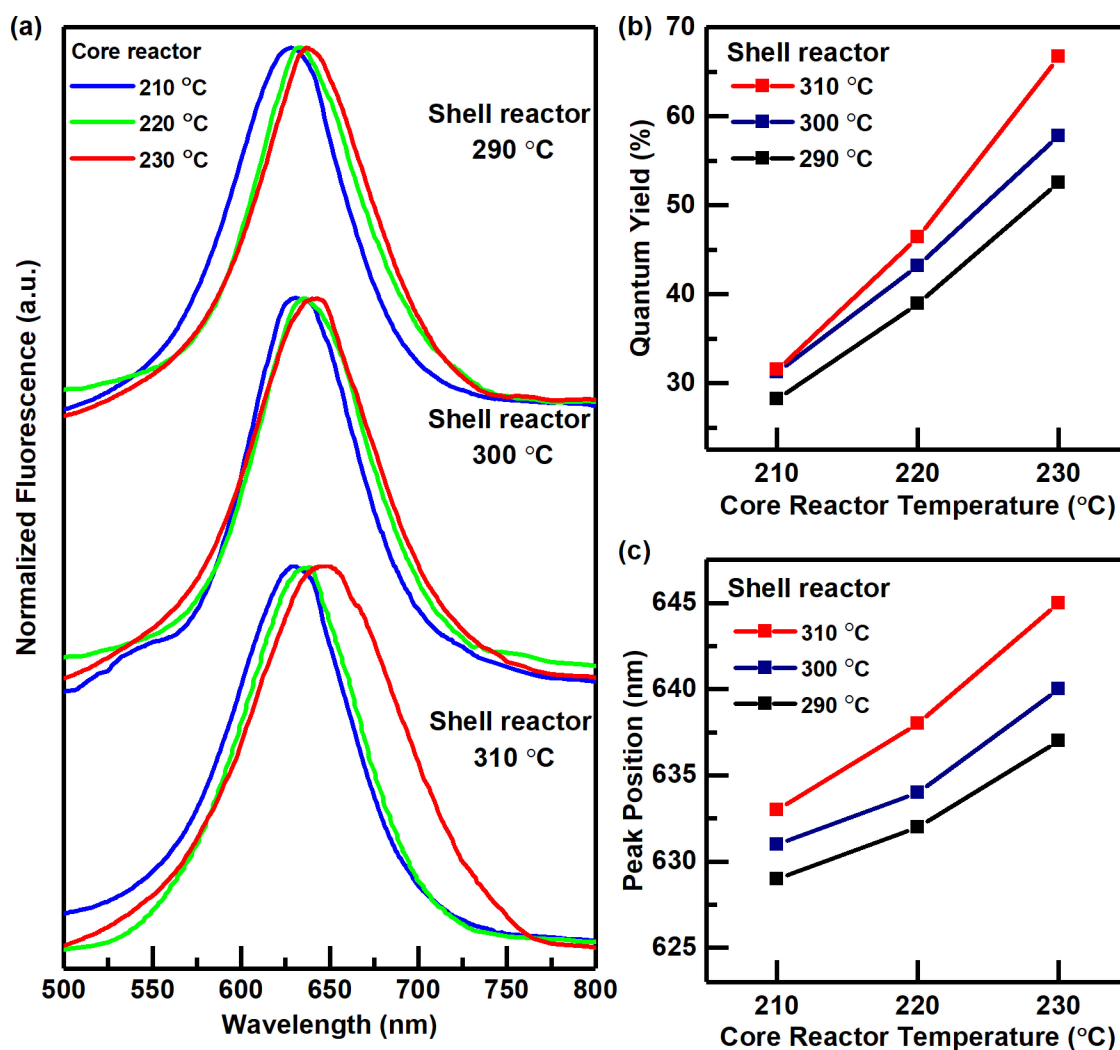


Figure 5. Effect of reactor temperature. (a) Normalized PL spectra, (b) Quantum Yield, and (c) Emission peak position for InP/ZnSeS synthesized at varying core and shell reactor temperatures. The shell reactor temperatures in (a) are shown adjacent to the spectra. The residence time in core reactor was kept at 45 minutes.

was increased from 210 to 230 °C while maintaining the shell growth temperature at 310 °C. A change in shell growth temperature instigates only a small effect on InP/ZnSeS PL characteristics and thus QY at lower core reactor temperature. One possible explanation that no significant change in the optical properties is observed upon changing the shell reactor temperature is that the low crystallinity of core particles at low core growth temperatures may become a bottleneck for shell passivation. To confirm this hypothesis, one would have to do a detailed InP core material characterization to quantify the crystallinity of the cores as a function of growth temperature.

Effect of shell precursor concentration: The photoluminescence of core-shell structures are known to be very sensitive to shell thickness.^[8b] Although changes in reactor temperature and flow rate also affect the extent of shell passivation, varying shell precursor concentration in the flow stream entering the shell reactor can be a very effective way to influence shell thickness. To optimize the shell precursor concentration leading to a high quality (i.e., high PL QY) InP/ZnSeS final product and to

understand the interplay between residence time and shell precursor concentration in the flow reactors, we varied the [Zn]:[In] ratio along with the residence time (Figure 6). The concentration of the shell precursors was varied by addition of solvent, while maintaining a constant relative molar ratio of Se, S, and Zn precursors (Se:S and Zn:(Se+S)). As expected, the PL spectra show a significant red shift upon increasing both the [Zn]:[In] ratio and the residence time due to increased shell passivation (Figure 6c). However, the [Zn]:[In] ratio shows a clear optimum PL QY at higher residence time (30 minute and 45 minute), and levels off for smaller residence time (Figure 6b). The increase in PL QY can be attributed to the growth of a thicker ZnSeS shell as a result of increased availability of shell precursors in the shell growth step. Figure S4 in the supporting information shows the increase in average diameter of InP/ZnSeS upon shell passivation of InP core particles (size: 3.8 ± 0.9 nm), synthesized at 45 minutes core residence time. The shell thickness increases from 0.9 nm ([Zn]:[In]=10:1) to 1.15 nm ([Zn]:[In]=25:1), exhibiting maximum PL QY at inter-

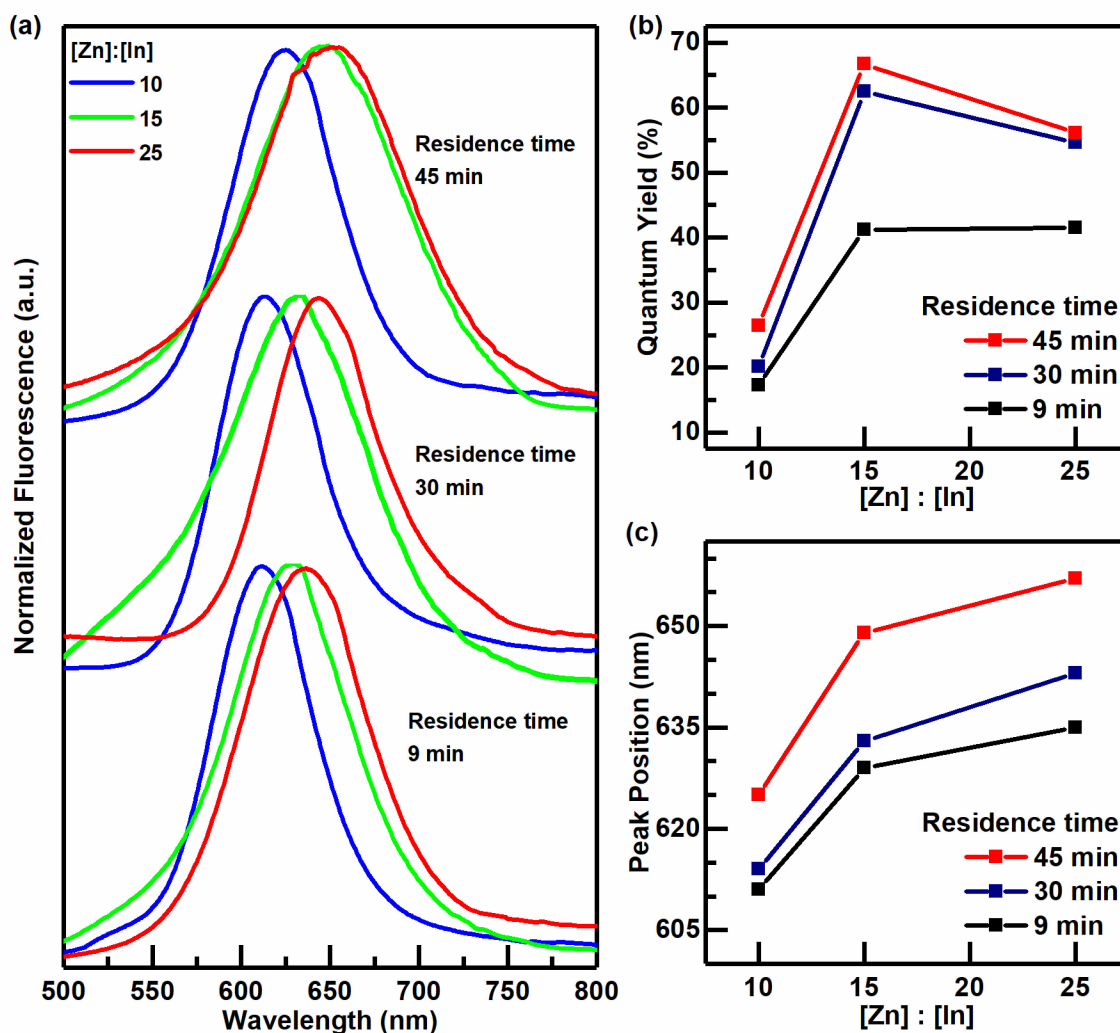


Figure 6. Effect of shell precursor concentration. (a) Normalized PL spectra, (b) Quantum Yield, and (c) Emission peak position for InP/ZnSeS synthesized at varying shell precursor concentration (shown as [Zn]:[In] ratio) at different residence time in core reactor. The residence time in (a) is shown adjacent to the spectra. The reactors were kept at 230 °C (core) and 310 °C (shell).

mediate shell concentration ([Zn]:[In]=15:1) with 1.05 nm shell thickness (Figure 4a). However, the standard deviation in the size of the InP/ZnSeS synthesized at different shell precursor concentrations, overlap with each other and hence the change in shell thickness are not statistically significant based on the TEM images alone. The increase in shell thickness can also be explained by the observed red shift in PL emission upon increasing the shell precursor concentration used (Figure 6 and Figure S2). Other complementary techniques like global EDX characterization can be used along with the TEM imaging to quantify the shell thickness and confirm its increase. The steep red-shift and drop in PL QY (Figure 6b) at [Zn]:[In] ratio of 15:1 is probably caused by the formation of a thicker shell up to a point where the increased strain at the core-shell interface induces a higher lattice mismatch, resulting into an appreciable decrease in quantum yield when the [Zn]:[In] ratio was further increased. However, at the lower residence time of 9 minutes, even in presence of a high shell precursor concentration, the shell thickness does not attain an optimum due to relatively

lower residence time, despite high shell precursor concentration and hence PL QY does not show a steep drop. In the case of pure ZnSe shell growth on a InP core, prior work has been shown that thick shells can be grown without sacrificing QY, possibly due to lower lattice mismatch.^[17] In the case of ZnSeS shell growth, ZnSe has been shown to selectively passivate compared to ZnS, due to a difference in precursor reactivity. Hence, the effect of increased overall shell precursor can be attributed to the increased ZnS fraction in the shell layer. Further elemental mapping of the synthesized nanoparticles with varying Se and S precursor has been previously reported for InP/ZnSeS nanostructures in detail.^[10a]

2.3.1. Analysis of DOE Results

After completing all DOE runs, we sought to analyze the combined effect of all four parameters studied on the PL wavelength and QY of QDs produced. As evident from the

graphs in Figure S2, the effect on PL QY based on each parameter is not linear and hence the parameters are interdependent. For instance, the same PL peak position and QY can be achieved by different sets of parameters. The reaction conditions yielding product with the highest PL QY are a core reactor temperature of 230 °C, shell reactor temperature of 310 °C and core growth residence time of 45 minutes. At longer residence times or higher growth reaction temperatures, larger sized InP/ZnSeS QDs exhibiting high PL QY are obtained, suggesting that the QD quality might be better for larger sizes. In the absence of the reaction conditions induced differences in the crystal quality, there can also be an optimum core/shell QDs size range that gives rise to higher PL QY. Smaller sizes have more confinement of carrier (and therefore better overlap of electron and hole wave functions that results in higher PL) but they also have shorter distances to the surface where non-radiative recombination can occur. The QDs synthesized at the intermediate shell thickness, induced by varying the shell precursor concentration ($[Zn]:[In]$) show a similar trend with maximum PL QY at $[Zn]:[In]$ ratio of 15:1. However, despite varying these process parameters systematically, a minimum FWHM of 72 nm (0.25 eV) was attained for low PL QDs, while for most of the nanoparticles that exhibited high PL quantum yield a FWHM of over 80 nm (0.26 eV) was observed. The occurrence of these rather broad spectra (large FWHM) can be attributed to the inhomogeneous growth of relatively large core-shell quantum dots emitting in the orange-red region (> 600 nm). Subsequent efforts would have to focus on the synthesis of smaller core-shell structures with reduced FWHM by preventing the over-ripening which in turn will improve the size distribution and overall product quality. Another approach to address the issue of poor control over core growth can be achieved by utilizing an alternate precursor-solvent combination. The presence of fatty acids in octadecene is known to be responsible for *in situ* formation of water at high temperature, which in turn may result in uncontrolled growth of an oxide layer around InP core particles, thus negatively affecting the shell passivation and the optical properties of the final product.^[28] Use of indium halides and aminophosphines in primary amines as solvent for InP QD synthesis can eliminate the possible oxidation of core particles.^[17]

2.4. Spanning the Visible Spectrum

As a next step, with the goal to span nearly the entire visible spectrum, we varied different process parameters (including concentration, both core and shell reactor temperatures and individual residence times) based on the trends observed in the DOE study. The core reactor was operated at 220 °C and a high flow rate (residence time of 2 minutes) of InP precursors with twice the amount of solvent, to obtain smaller core particles. However, with a decreased residence time, the overall precursor conversion in the reactor also decreased and hence a purification step to remove the unreacted precursors from the core product before the shell growth step became inevitable. To make the system fully continuous for even lower residence

times (while avoiding the need for purification of the core product through conventional benchtop methods), future efforts would need to focus on integration of inline purification modules before the shell growth. For example, recently a multistage extraction platform for inline purification of nanoparticles has been reported, which holds potential for purification in continuous flow system designs.^[29] After core product formation and purification, the purified product was introduced to the mixer unit to initiate shell growth. Based on the blue-shift trend observed in the InP/ZnSeS PL spectrum upon decreasing the $[Zn]:[In]$ ratio (Figure 6), we reduced the $[Zn]:[In]$ ratio even further to 5:1 (Figure 6). Using this $[Zn]:[In]$ ratio while varying the shell growth residence time from 6 to 9 and then to 45 minutes, we obtained InP/ZnSeS products emitting at 486 nm, 514 nm, and 551 nm (blue – green region) respectively (see Figure 7), indicating that particles with thicker

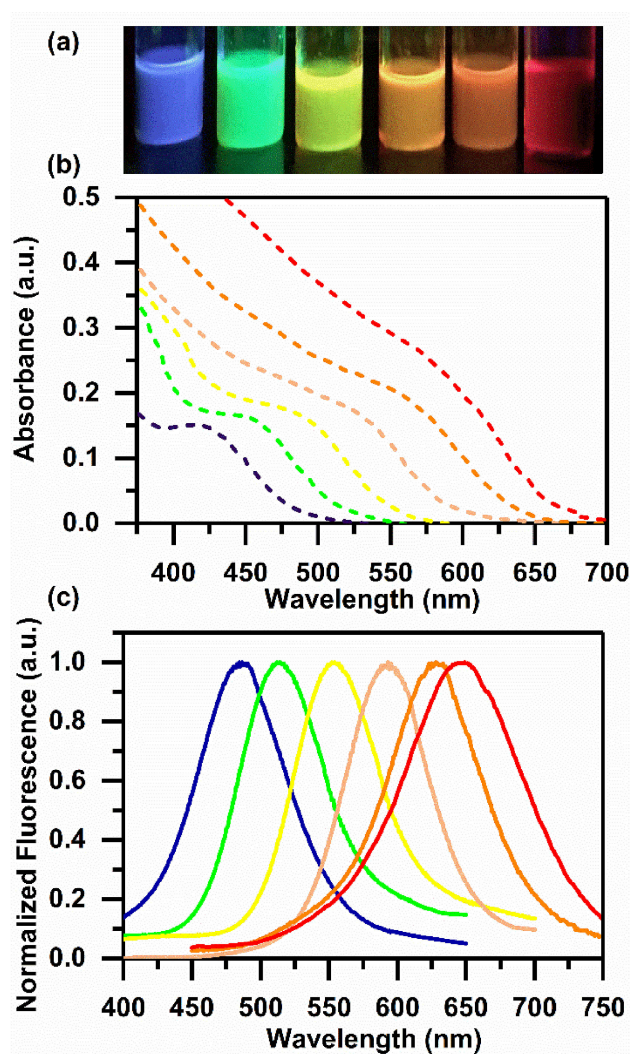


Figure 7. Tuning parameters to cover the visible spectrum. (a) Image of as-synthesized InP/ZnSeS product solutions under UV-light. (b) Absorbance and (c) Normalized fluorescence spectra of the different InP/ZnSeS products. All spectra are uniformly color coded with their emission wavelength color.

shells were synthesized. However, the entire visible spectra cannot be spanned by merely varying the shell passivation time and hence in order to achieve particles emitting at higher wavelengths, the core size was further tuned. For achieving particles emitting in the orange-red region, the core size was increased by increasing both the residence time from 2 minutes to 9–45 minutes (depending on emission wavelength) as well as the reactor temperatures. The exact reaction conditions for a product exhibiting an emission wavelength >600 nm are shown in the complete DOE results (Figure S2).

The demonstrated ability to synthesize InP/ZnSeS quantum dots that cover nearly the entire visible spectrum shows that the two-stage modular continuous flow reactor setup used here can systematically tune the PL properties of QDs. Note however, that the PL QY of the InP/ZnSeS particles, especially those emitting in the blue-yellow region (PLQY $<25\%$), needs further improvement. A new DOE study, similar to what was conducted for particles emitting at longer wavelengths (>600 nm), is recommended to further enhance the PL properties for particles emitting in the blue-green region.

2.5. Production Rate Analysis

A major advantage of using millifluidic reactors rather than microfluidic reactors for nanoparticle synthesis is the ability to produce high quality nanoparticles at high production rate for large scale synthesis.^[22,24,25b] The overall reaction yield in our millifluidic reactor set up ranges from 60 to 80% based on calculation for three different flow rate conditions. It certainly depends on the reaction conditions (growth temperature and flow rate) and precursor concentrations. However, as expected the product obtained contains a high amount of unreacted Zn precursors. Despite this high Zn precursor concentration, no evidence of secondary nucleation was observed in the UV-Vis/PL spectra or the TEM images of the final product. One explanation for this lack of secondary nucleation can be that even at high Zn:In ratio, the concentration of Se and S precursors are still below the threshold for secondary nucleation. We determined the actual production rate for two InP/ZnSeS products. The respective product solutions were collected and centrifuged in a mixture of methanol and ethanol, and dried to obtain the powdered nanoparticles. Continuous flow synthesis using a residence time of 9 minutes resulted InP/ZnSeS quantum dots exhibiting 40% PL QY (emission peak position = 628 nm) at a production rate of 186 mg/hour (equivalent to 4.4 g/day) using a single-channeled reactor. Performing the synthesis with a 30 minute residence time yielded nanoparticles at a rate of 109 mg/hour. Higher production rates could be achieved by stacking multiple channels in parallel, as reported previously for microfluidic reactors.^[20] Similarly, the stainless steel reactor modules used in our study can easily be modified to contain multiple reaction channels that all experience similar reaction conditions (temperature, residence times, heat and mass transfer rates, etc.). For instance, with around 20–25 reactor channels within the same reactor module, the nanoparticles exhibiting high PL QY can be produced at rate

exceeding 100 g/day, a level of interest for commercial production. Understanding the extent of heat and mass transfer control in the multichannel configurations would, however, be essential to ensure large-scale production of QDs with narrowly defined optical properties.

The product stream containing crude QD solution includes excess amount of ligands and unreacted precursors that needs to be effectively removed before application of these synthesized QDs. This post-synthetic purification is typically carried out using a precipitation-dissolution method followed by centrifugation in a batch-wise fashion, that is time consuming and inefficient for large-scale application. The modular continuous flow reactor setup reported here is still limited in that it lacks the ability of post-synthetic purification in continuous fashion. The exploration of possible post-synthetic treatments inline with a continuous flow synthesis platform is still an emerging area of research. For example, a multistage extraction platform has been reported, that implements a continuous flow liquid-liquid extraction system to purify synthesized quantum dots.^[29] Similarly, Jeong et al. recently reported continuous purification platforms utilizing porous electrodes in a flow channel.^[30] Indeed, integration of continuous purification modules with continuous flow synthesis platforms may yield an even more efficient fully-continuous manufacturing platform for different nanomaterials.

3. Conclusions

In summary, we demonstrated successful application of a modular continuous flow millifluidic reactor setup for multistep synthesis of highly luminescent InP/ZnSeS core-shell QDs. The particles exhibited PL QY as high as 67%, exceeding previously reported for Cd-free particles obtained via continuous flow synthesis by a factor of up to three.^[19b,d,21,25a] The modular design of the setup used in our study allowed for precise control over rapid and uniform heating, cooling, and mixing of the flow streams, which appear to be crucial in obtaining nanoparticles with narrowly defined optical characteristics. The modular setup also enabled a systematic parameter sensitivity study which enhanced our understanding of the relative importance of different process parameters in enhancing PL of the InP/ZnSeS QDs. This understanding allowed for the targeted synthesis of a range of particles whose emission wavelengths span the entire visible spectrum (480–650 nm). Moreover, high production rates (>100 mg/h/single channel) of particles that exhibit PL QY as high as 62% can be achieved. This demonstrated ability to synthesize QDs with high production rate without compromising product quality underscores the promise of continuous flow millifluidic reactor setups for production of nanoparticles with desired optical properties at large scales.

Looking ahead, one can also foresee application of the modular millifluidic reactor platform for the synthesis of core-shell QDs of different compositions or of more complex heterostructures. Indeed, it has potential as a versatile system for screening a wide range of compositions and structures in

relation to desired optical or catalytic properties. Moreover, the continuous flow system can be enhanced further by integration of inline purification or optical characterization modules. The latter would provide real-time information about progression of particle growth, which is crucial for growth kinetics studies, and can provide an avenue for product optimization via feedback process control.

Experimental Section

Chemicals: Indium acetate (99.5%), Myristic acid (Sigma grade, >99%), octadecene (ODE) (technical grade, 90%), oleic acid (90%), trioctylphosphine (TOP) (90%), selenium (99.99%), 1-dodecanethiol (DDT) (> 98%) and Zn-acetate were purchased from Sigma-Aldrich and used as received. Tris(trimethylsilyl)phosphine (TMSP) (> 98%) was purchased from Strem Chemical and used as received.

Indium myristate (0.1 M) stock solution: 2 mmol of In-acetate was heated with 6 mmol myristic acid in a three-neck flask with 20 mL Octadecene under vacuum for one hour at 120 °C to obtain a clear Indium myristate solution. The solution was stored in glovebox after sufficient degassing.

TOP-Se (1M) stock solution: TOP-Se was prepared by sonicating 20 mmol of Se in 20 mL of TOP until a clear and well-dissolved TOP-Se solution was obtained. The stock solution was transferred to glovebox after degassing for around one hour.

Precursor preparation: For a typical synthesis, 0.2 mmol of Zn-acetate, 0.4 mmol of oleic acid, and 16 mL of octadecene were stirred under inert atmosphere in a three-neck flask (InP precursor flask) equipped with a condenser. The mixture was then heated to 120 °C under vacuum until Zn-acetate dissolved completely in octadecene (typically 45 minute). In a separate 3-neck flask (ZnSeS precursor flask), typically, 3 mmol of Zn-acetate, 6 mmol of oleic acid, and 18.6 mL of ODE was heated to 120 °C under vacuum until Zn-acetate dissolved completely in octadecene (typically 45 minute). Both the flasks were purged with nitrogen, followed by two vacuum-nitrogen cycles (1 cycle = 15 minute vacuum + 1 minute nitrogen). Finally, the temperature of the InP precursor solution was brought down to 50 °C and both flasks were kept under nitrogen pressure of 5 psig.

InP/Zn synthesis in the core reactor: The entire reactor setup was kept under vacuum (30 minutes) and then purged with nitrogen (15 minutes) to remove oxygen in the setup. Following the nitrogen purge, the setup (including the three-neck flasks) was then maintained at a positive pressure of about 5 psig to avoid any back diffusion of air. 2 ml (0.2 mmol) of Indium myristate stock solution was premixed with 0.2 mmol of TMSP and 2 ml of octadecene in a glovebox. The solution quickly changed in color to pale yellow indicating the formation of InP nuclei. The pre-mixed solution containing InP nuclei was then transferred to the InP-flask under inert conditions to avoid oxidation of the nuclei. The well-mixed InP precursor mixture was pumped into the first reactor (core reactor) set at 230 °C (or desired temperature) at specified flow rate (typically equivalent residence time of 2–45 minute) by a peristaltic pump. The Zn(OA)₂-passivated InP product stream coming from core reactor was cooled down by the cooling module installed downstream of the reactor for quickly bringing temperature back to room temperature to avoid any unwanted residual reaction.

ZnSeS shell growth in the shell reactor: Typically, 0.3 mL of TOP-Se and 1.1 mL of DDT was added to the ZnSeS precursor flask kept at 120 °C under inert conditions. Once the InP core product stream

started approaching the static mixer, the second pump was turned on to pump the precursor mixture from the ZnSeS-flask at the desired flow rate. The two streams (product from the core reactor and the precursors from the ZnSeS-flask) mixed well as they flowed through the static mixer into the second reactor. The static mixer was kept at 90 °C along with the shell precursor flow tubes (to avoid solidification of precursors). The temperature for the second reactor (shell reactor) was set at 310 °C (or the desired temperature). The final product with shell passivated core-shell particles left the second cooling module attached downstream of the reactor. The product was collected in an air tight product vial kept under Nitrogen with a back pressure of 5 psig. The entire process from core precursor entering the first reactor, up to the first product stream in the product vial takes a total of nearly 2.5 times the core residence time (depending on the operating flow rate). The product stream exiting after one core residence time into the product vial is collected for characterization of the core-shell QDs. From multiple prior runs we confirmed that steady-state operation always is attained sometime before one core residence time has passed.

Characterization of quantum dots: The as-synthesized product solution was typically diluted 1:30 in chloroform to obtain an absorbance between 0.02 and 0.05 at 495 nm. Absorption spectra were obtained from an 8453 UV-Vis Diode Array System spectrophotometer (Agilent) and PL spectra were obtained from a Jobin-Yvon Fluoromax-3 spectro-fluorometer (Horiba); the excitation wavelength varied between 385 and 495 nm depending on the particles synthesized. For particles in orange-red region, 495 nm excitation wavelength was used and PL QY were determined by comparing intensities to a standard dye solution of Rhodamine 6G (in ethanol, 95% QY) with similar optical density at the excitation wavelength. The sample with highest PL QY was confirmed (deviation of less than 3%) by absolute QY measurement obtained from a Horiba Jobin-Yvon Nanolog spectro-fluorometer equipped with an integrating sphere. Transmission electron microscopy (TEM) was carried out on a JEOL 2010 LaB₆ TEM. For TEM, 1 mL of the product sample was centrifuged in a 30 mL mixture of ethanol and methanol (1:1). The precipitate was dissolved in chloroform and applied to a carbon-coated copper grid for TEM imaging.

System module components: The stainless-steel reactors and cooling modules were fabricated using conventional machining techniques. The helical static mixers were purchased from Omega (FMX 84442S). Cartridge heaters (4-inch-long) used for reactor heating have power rating of 60 W (purchased from McMaster Carr). The entire reactor module was insulated using a layer of ceramic wool and a layer of ceramic roll (Unifrax LLC). The custom-designed inline mixer present between the reactor modules, consist of 5 Sulzer SMX plus mixing elements (each 4.8 mm wide and 4.8 mm long), and was purchased from Stamixco. The precursor was flowed into the reactors at a set flow rate (ranging from 0.1 mL/min to 1.5 mL/min) using a Masterflex peristaltic pump with Teflon tubing. The EDS analysis of a typical sample obtained using the current reactor system does not show presence of any significant amount of contaminants due to possible leaching from the stainless steel wall of the reactor (Figure S7 in the SI).

Acknowledgements

We gratefully acknowledge financial support from the Dow Chemical Company for research agreement #226772AC. We thank D. Guironnet for providing access to a glove box. We acknowledge the contribution of Y. Zhai, G. Drake and the Dow research team for stimulating discussions. We also thank M.

Harland for his input on fabrication of the reactor set up. TEM imaging was carried out in the Frederick Seitz Materials Research Laboratory Central Research Facilities, University of Illinois.

Conflict of Interest

The authors declare no conflict of interest.

Keywords: quantum dots · continuous flow · millifluidic reactors · indium phosphide · cadmium free

- [1] a) A. Beveratos, I. Abram, J. M. Gerard, I. Robert-Philip, *Eur. Phys. J. D* **2014**, *68*, 377; b) N. Oh, S. Nam, Y. Zhai, K. Deshpande, P. Trefonas, M. Shim, *Nat. Commun.* **2014**, *5*, 3642.
- [2] a) R. M. Crooks, M. Q. Zhao, L. Sun, V. Chechik, L. K. Yeung, *Acc. Chem. Res.* **2001**, *34*, 181; b) H. Tada, T. Kiyonaga, S. Naya, *Chem. Soc. Rev.* **2009**, *38*, 1849; c) W. J. Yin, S. Bai, Y. J. Zhong, Z. Q. Li, Y. Xie, *ChemNanoMat* **2016**, *2*, 732; d) Q. Zhu, W. L. Chen, F. Dai, Y. P. Yuan, X. Y. Wu, J. T. Zai, R. R. Qi, X. F. Qian, *ChemNanoMat* **2015**, *1*, 52.
- [3] a) M. Bally, J. Voros, *Nanomedicine* **2009**, *4*, 447; b) A. Ito, M. Shinkai, H. Honda, T. Kobayashi, *J. Biosci. Bioeng.* **2005**, *100*, 1; c) Y. H. Lin, K. Nienhaus, G. U. Nienhaus, *ChemNanoMat* **2018**, *4*, 253.
- [4] a) C. D. Donega, P. Liljeroth, D. Vanmaekelbergh, *Small* **2005**, *1*, 1152; b) H. M. Pathan, B. R. Sankapal, J. D. Desai, C. D. Lokhande, *Mater. Chem. Phys.* **2003**, *78*, 11; c) L. W. Liu, S. Y. Hu, Y. Pan, J. Q. Zhang, Y. S. Feng, X. H. Zhang, *Beilstein J. Nanotechnol.* **2014**, *5*, 919.
- [5] R. Hardman, *Environ. Health Perspect.* **2006**, *114*, 165.
- [6] M. J. Anc, N. L. Pickett, N. C. Gresty, J. A. Harris, K. C. Mishra, *J. Sci. Technol.* **2013**, *2*, R3071.
- [7] A. Thomas, P. V. Nair, K. George Thomas, *J. Phys. Chem. C* **2014**, *118*, 3838.
- [8] a) L. Li, P. Reiss, *J. Am. Chem. Soc.* **2008**, *130*, 11588; b) X. Y. Yang, D. W. Zhao, K. S. Leck, S. T. Tan, Y. X. Tang, J. L. Zhao, H. V. Demir, X. W. Sun, *Adv. Mater.* **2012**, *24*, 4180; c) S. Joung, S. Yoon, C. S. Han, Y. Kim, S. Jeong, *Nanoscale Res. Lett.* **2012**, *7*, 1.
- [9] K. Kim, H. Lee, J. Ahn, S. Jeong, *Appl. Phys. Lett.* **2012**, *101*, 073107.
- [10] a) J. Lim, W. K. Bae, D. Lee, M. K. Nam, J. Jung, C. Lee, K. Char, S. Lee, *Chem. Mater.* **2011**, *23*, 4459; b) J. Lim, M. Park, W. K. Bae, D. Lee, S. Lee, C. Lee, K. Char, *ACS Nano* **2013**, *7*, 9019.
- [11] S. Kim, J. Park, T. Kim, E. Jang, S. Jun, H. Jang, B. Kim, S. W. Kim, *Small* **2011**, *7*, 70.
- [12] S. Koh, T. Eom, W. D. Kim, K. Lee, D. Lee, Y. K. Lee, H. Kim, W. K. Bae, D. C. Lee, *Chem. Mater.* **2017**, *29*, 6346.
- [13] D. K. Harris, M. G. Bawendi, *J. Am. Chem. Soc.* **2012**, *134*, 20211.
- [14] D. C. Gary, B. M. Cossairt, *Chem. Mater.* **2013**, *25*, 2463.
- [15] L. Li, M. Protiere, P. Reiss, *Chem. Mater.* **2008**, *20*, 2621.
- [16] E. Bang, Y. Choi, J. Cho, Y. H. Suh, H. W. Ban, J. S. Son, J. Park, *Chem. Mater.* **2017**, *29*, 4236.
- [17] M. D. Tessier, D. Dupont, K. De Nolf, J. De Roo, Z. Hens, *Chem. Mater.* **2015**, *27*, 4893.
- [18] S. Tamang, C. Lincineau, Y. Hermans, S. Jeong, P. Reiss, *Chem. Mater.* **2016**, *28*, 2491.
- [19] a) A. M. Nightingale, J. C. de Mello, *ChemPhysChem* **2009**, *10*, 2612; b) J. Baek, P. M. Allen, M. G. Bawendi, K. F. Jensen, *Angew. Chem. Int. Ed.* **2011**, *50*, 627; c) M. Abolhasani, C. W. Coley, L. S. Xie, O. Chen, M. G. Bawendi, K. F. Jensen, *Chem. Mater.* **2015**, *27*, 6131; d) L. S. Xie, D. K. Harris, M. G. Bawendi, K. F. Jensen, *Chem. Mater.* **2015**, *27*, 5058.
- [20] A. M. Nightingale, J. C. de Mello, *J. Mater. Chem.* **2010**, *20*, 8454.
- [21] L. S. Xie, Y. Shen, D. Franke, V. Sebastian, M. G. Bawendi, K. F. Jensen, *J. Am. Chem. Soc.* **2016**, *138*, 13469.
- [22] S. Biswas, J. T. Miller, Y. H. Li, K. Nandakumar, C. S. S. R. Kumar, *Small* **2012**, *8*, 688.
- [23] R. Gottesman, A. Tangy, I. Oussadon, D. Zitoun, *New J. Chem.* **2012**, *36*, 2456.
- [24] S. E. Lohse, J. R. Eller, S. T. Sivapalan, M. R. Plews, C. J. Murphy, *ACS Nano* **2013**, *7*, 4135.
- [25] a) K. Kim, S. Jeong, J. Y. Woo, C. S. Han, *Nanotechnology* **2012**, *23*, 065602; b) M. S. Naughton, V. Kumar, Y. Bonita, K. Deshpande, P. J. A. Kenis, *Nanoscale* **2015**, *7*, 15895; c) V. Kumar, H. A. Fuster, N. Oh, Y. Zhai, K. Deshpande, M. Shim, P. J. A. Kenis, *ChemNanoMat* **2017**, *3*, 204.
- [26] a) R. Xie, Z. Li, X. Peng, *J. Am. Chem. Soc.* **2009**, *131*, 15457; b) P. M. Allen, B. J. Walker, M. G. Bawendi, *Angew. Chem. Int. Ed.* **2010**, *49*, 760.
- [27] S. Hirschberg, R. Koubek, F. Moser, J. Schock, *Chem. Eng. Res. Des.* **2009**, *87*, 524.
- [28] H. Virieux, M. Le Troedec, A. Cros-Gagneux, W. S. Ojo, F. Delpech, C. Nayral, H. Martinez, B. Chaudret, *J. Am. Chem. Soc.* **2012**, *134*, 19701.
- [29] Y. Shen, N. Weeranoppanant, L. Xie, Y. Chen, M. R. Lusardi, J. Imbrogno, M. G. Bawendi, K. F. Jensen, *Nanoscale* **2017**, *9*, 7703.
- [30] H. Lim, J. Y. Woo, D. C. Lee, J. Lee, S. Jeong, D. Kim, *Sci. Rep.* **2017**, *7*, 43581.

Manuscript received: April 10, 2018
Accepted Article published: June 29, 2018
Version of record online: July 19, 2018